# Overdamped Brownian Dynamics in a Potential Trap under a Nonuniform Temperature Field

Cin-Hua Pan[1](潘勤華) and Pik-Yin Lai*[1,2](黎璧賢)

[1]*Department of Physics and Center for Complex Systems, National Central University, Chung-Li District, Taoyuan City 320, Taiwan, R.O.C. and*

[2]*Physics Division, National Center for Theoretical Sciences, Taipei 10617, Taiwan, R.O.C.*

(Dated: September 3, 2025)

## Abstract

We investigate the dynamics and statistics of a one-dimensional Brownian particle in a potential trap under a spatially non-uniform temperature field. For single minimum harmonic or anharmonic trapping potentials and unimodal temperature field, the Brownian particle can be described by a double-well effective potential with an effective barrier, with the effective potential and the steady-state position distribution derived analytically using the Fokker-Planck equation. The transition rate between the two wells in the effective potential is also derived. In addition, the impact of a nonuniform temperature on the escape kinetics in a double-well potential is also considered with the modified transition rate derived analytically, indicating a suppression of the energy barrier and hence an enhancement of the transition rate between the two wells. Furthermore, it is demonstrated that a tilted double-well effective potential can be obtained by mismatching the centers of the trapping well and the temperature profile, opening the possibility of constructing a memory erasure device in such a system. The nonequilibrium nature due to the temperature gradient is also discussed in terms of the hidden entropy production, as revealed by the corresponding underdamped dynamics. Numerical simulations of the corresponding Langevin dynamics verify all of these theoretical results.

* pylai@phy.ncu.edu.tw

## INTRODUCTION

Typical equilibrium systems are characterized by a spatially uniform temperature with no temperature differences or gradients[1]. However, temperature gradients are ubiquitous in practice in open systems as a result of the presence of localized heat sources. The spatially non-uniform temperature field inevitably leads to heat flux that can give rise to non-equilibrium behavior. In many situations, spatially nonuniform temperature is characterized by a time-independent temperature field in which temperature reservoirs can be created at different temperatures or by localized heating sources. The temperature gradient can often give rise to a spatially non-uniform diffusion field or, in some cases, give rise to thermophoretic effects[2] that result in a net particle flux due to the non-uniform thermal fluctuations, manifesting the non-equilibrium nature[3].

One of the simplest cases of spatially non-uniform temperature is having a hot and a cold reservoir in different locations. As early as 1912, Smoluchowski proposed the Brownian ratchet [4] thought experiment, which was later popularized by Richard Feynman[5]. The famous Feynman ratchet[6] consisted of two heat reservoirs connected by a paddle. A gear in one of the reservoirs can only rotate in one direction due to the ratchet constraint, and the paddle in the other reservoir can only turn in a single direction due to the Brownian bombardment. As long as there is a temperature difference between the two heat reservoirs, the work done by rotating the gear does not violate the second law of thermodynamics. Subsequently, Büttiker[7] and Laudauer[8] proposed the Büttiker-Laudauer motor which is simply an overdamped Brownian particle moving in a spatially periodic potential but subjected to a spatially inhomogeneous temperature. Another example of a non-equilibrium system consisting of two distinct temperatures is the autonomous Brownian gyrator[9–11], which has been demonstrated experimentally and theoretically under two uniform temperatures acting on two different degrees of freedom. However, the autonomous Brownian gyrator cannot extract useful work.

The Brownian particle [12–14] under a trapping potential remains a paradigm system for investigating many interesting equilibrium and nonequilibrium stochastic systems under thermal fluctuations. Such a system can be well described and often tackled analytically by the Fokker-Planck equation[15] and the Langevin equation[16], with the associated energetics in the mesoscale quantitatively described by stochastic thermodynamics[17, 18].

In particular, the Fokker-Planck equation approach provides the theoretical framework for calculating the stochastic transitions between different metastable states.

The study of transition rates in stochastic systems is a fundamental topic in statistical physics, with broad applications in chemical kinetics, condensed matter physics, and biological processes. The seminal work of Kramers [19] laid the foundation for understanding the escape rate of a Brownian particle from a metastable state under thermal fluctuations. This theory describes how a particle can overcome an energy barrier in the presence of thermal noise, with the escape rate depending on both the height of the potential barrier and the damping properties of the medium. In general, the transition rate decreases exponentially with the barrier height, which can be simply understood as the Arrhenius equation in chemistry, where the activation energy is the barrier. Traditional formulations of transition rates often assume a uniform temperature field, where the thermal noise is spatially homogeneous. On the other hand, there are few studies on the transition rate over an energy barrier at nonuniform temperature[7, 19]. However, many real-world systems exhibit spatially varying temperature or diffusion profiles[20, 21], which can lead to modifications of noise strength and escape dynamics. It would be desirable to have a system in which the energy barrier can be manipulated in a controlled fashion, and hence the transition rates can be tuned conveniently.

In this paper, we examine the behavior of an overdamped one-dimensional Brownian particle trapped in a potential under a spatially non-uniform temperature field. The effective potential experienced by the Brownian particle is derived using the Fokker-Planck equation and is shown to have a double-well structure. The transition rate between the two wells in the effective potential is then investigated analytically. The impact of spatially varying temperature fields on the transition rates of a Brownian system is explored by extending the classical Kramers approach. It is demonstrated that a Brownian particle under a trapping potential can experience an effective potential with an energy barrier in the presence of a spatially non-uniform temperature field. The effective energy barrier depends on the temperature profile, thus allowing the possibility of manipulating the effective energy barrier, and hence, the transition rates can be manipulated by applying a designed heating profile. The corresponding underdamped dynamics is also examined, revealing the nonequilibrium nature due to the temperature gradient as exemplified by the hidden entropy production.

## OVERDAMPED BROWNIAN PARTICLE TRAPPED IN A POTENTIAL UNDER SPATIALLY NON-UNIFORM TEMPERATURE AND DAMPING

We consider the overdamped dynamics of a one-dimensional Brownian particle in a potential trap $U(x)$ with spatially non-uniform temperature $T(x)$ and damping coefficient $\gamma(x)$. In this case, the Fokker-Planck equation reads[15, 17, 22]:

$$\frac{\partial P(x,t)}{\partial t} = -\frac{\partial J(x,t)}{\partial x}, \tag{1}$$

$$J(x,t) \equiv -\frac{1}{\gamma(x)}\left[U'(x)P(x,t) + \frac{\partial}{\partial x}\left(k_B T(x) P(x,t)\right)\right] \tag{2}$$

where $P(x,t)$ is the probability density of the Brownian particle at time $t$, $J(x,t)$ is the flux, and the $'$ denotes the derivative with respect to $x$. The spatial dependence in $T$ or $\gamma$ leads to the multiplicative nature of the noise in the corresponding Langevin equation, which is given by[17]

$$\dot{x} = -\frac{1}{\gamma(x)}\frac{\partial U(x)}{\partial x} + k_B T(x)\frac{\partial}{\partial x}\frac{1}{\gamma(x)} + \sqrt{\frac{2k_B T(x)}{\gamma(x)}}\cdot\xi(t), \tag{3}$$

where $\xi$ is the standard zero-mean unit variance Gaussian white noise, with the noise term adopting the Itô product.

### Steady-state distribution and Effective potential

In the one-dimensional case, the spatial gradients in $T(x)$ or $\gamma(x)$ give rise to a drift force that competes with the potential force. Because of the confining nature of the potential trap in one dimension, one expects that the Brownian particle can be described by an effective potential energy similar to the equilibrium situation when the potential force balances with the drift forces. The steady-state solution of equation (1) is $J$ = constant. However, since the trapping potential limits the particle from going to $\pm\infty$, implying that $J = 0$ at $x \to \pm\infty$ and hence $J = 0$ everywhere, resulting in a steady state with no net particle flux. It should be noted that although there is no net flux for the Brownian particle, the system is not at thermodynamic equilibrium due to the non-uniform time-independent temperature profile, which gives rise to a non-vanishing steady-state heat flux. The heat transport for the Brownian particle under a nonuniform temperature field can be calculated using the stochastic energetics method[23].

From (2), the steady state particle distribution is given by

$$U'(x)P_{ss}(x) + \frac{\partial}{\partial x}\left(k_B T(x) P_{ss}(x,t)\right) = 0. \tag{4}$$

Direct integration of (4) gives the steady-state particle distribution

$$P_{ss}(x) = \frac{1}{Z}\frac{e^{-\int^x \frac{U'(y)}{k_B T(y)}dy}}{k_B T(x)} = \frac{1}{Z} e^{-\int^x \frac{U'(y)+k_B T'(y)}{k_B T(y)}dy}, \tag{5}$$

where $Z$ is the normalization constant. Therefore, one can define an effective potential as

$$U_{eff}(x) \equiv \tilde{T}\int^x \frac{U'(y) + k_B T'(y)}{T(y)}dy \tag{6}$$

where $\tilde{T}$ is some fixed constant temperature, for instance, one can choose $\tilde{T} = T(0)$ or $T(\infty)$. Therefore, in the presence of a nonuniform temperature field, the one-dimensional Brownian particle achieves a non-Boltzmann steady-state distribution. It is easy to see from (2) that when $T$ is independent of $x$, $P_{ss}(x)$ reduces to the usual Boltzmann distribution, even though the damping coefficient $\gamma(x)$ is spatially dependent.

Hereafter, we shall focus on the case of a uniform damping coefficient ($\gamma$), but the temperature is a function of position. The temperature field can be thought of as the spatially dependent profile $T(x)$ due to some localized heating, and $T(x \to \infty) \equiv T_\infty$ is the ambient temperature far away from the heating source. In this situation, the Langevin equation (3) reads

$$\gamma\dot{x} = -U'(x) + \sqrt{2\gamma k_B T(x)}\cdot\xi(t). \tag{7}$$

As illustrated in the following, the system can be put in dimensionless form by choosing appropriate units of length and time. The dimensionless effective potential, with $U_{eff}(0)$ taken to be zero, can be derived from (6) to be

$$U_{eff}(x) \;=\; \int_0^x \frac{U'(y) + T'(y)}{T(y)}dy \tag{8}$$

Hereafter, we focus on the case of a symmetric trapping potential with $U(-x) = U(x)$ and first consider the case of localized and symmetric heating applied at $x = 0$ (say a laser heating spot focused at $x = 0$) resulting in a symmetric temperature profile $T(-x) = T(x)$ that peaks at $x = 0$ with $T'(0) = 0$, $T''(0) < 0$ and $T(x \to \pm\infty) = T_\infty$ =constant. Then from (8), one has $U'_{eff}(0) = 0$ and $U''_{eff}(0) = \frac{U''(0)+T''(0)}{T(0)}$. Hence, the effective potential can have a local peak at $x = 0$, (i.e. a barrier at the origin) if $T''(0) < -U''(0)$.

**Brownian particle in a single-well trap and a unimodal temperature profile: transition in a double-well $U_{eff}(x)$**

We now consider the case of smooth symmetric single-well trapping potentials centered at the origin, which in general can be expressed in the form

$$U(x) = \frac{\lambda x^n}{2}, \quad n = 2, 4, 6, \cdots \tag{9}$$

where $\lambda$ is a constant controlling the potential strength. For convenience, we choose the length unit and time units respectively as $\left(\frac{k_B T_\infty}{\lambda}\right)^{1/n}$ and $\frac{\gamma}{k_B T_\infty}\left(\frac{k_B T_\infty}{\lambda}\right)^{2/n}$, then the energy and temperature are in units of $k_B T_\infty$ and $T_\infty$ respectively. Then all theoretical analysis and numerical simulation of the Langevin equation can be carried out in a dimensionless fashion. The dimensionless potential trap is simply $U(x) = x^n/2$, and the (dimensionless) effective potential can be obtained from (8) as

$$U_{eff}(x) \;=\; \frac{n}{2}\int_0^x \frac{y^{n-1}}{T(y)}dy + \ln\left[\frac{T(x)}{T(0)}\right], \quad n = 2, 4, 6, \cdots \tag{10}$$

As pointed out in the previous section, the effective potential has a double-well structure if $U''(0) < |T''(0)|$, with the wells located at $x = \pm w$ satisfying the following equation

$$U'_{eff}(w) = U'(w) + T'(w) = 0, \quad U''_{eff}(w) > 0. \tag{11}$$

To investigate the transition rates between the two wells, we place the Brownian particle at the left well at $x = -w$ and wait for thermal fluctuations to bring it to $x = 0$ for the first time. The dimensionless mean first-passage time of the particle, $\tau$, can be obtained by solving the dimensionless backward Fokker-Planck equation [19].

$$\left[-\frac{\partial U}{\partial x} + T(x)\frac{\partial}{\partial x}\right]\frac{\partial}{\partial x}\tau(x) = -1. \tag{12}$$

The solution of $\tau$ at $x = -w$ gives the inverse of the transition rate as

$$K^{-1} \equiv \tau(-w) = \frac{T_\infty}{T_0}\int_{-w}^{0} dy \int_{-\infty}^{y} e^{G(x,y)}dx \equiv \frac{T_\infty}{T_0}K_0^{-1}, \tag{13}$$

where $K_0$ represents the transition rate at the ambient temperature $T_\infty$, and

$$G(x, y) \equiv \int_0^y \frac{U'(s)}{T(s)}ds - U_{eff}(x). \tag{14}$$

It can be shown that $(\pm w, 0)$ are always saddle points of $G(x, y)$. Hence, the saddle-point approximation can be applied to evaluate the integral in (13) to give an explicit approximate expression for $K$.

For further explicit calculations, we consider the dimensionless Gaussian temperature profile

$$T(x) = 1 + \Delta \exp\left(-\frac{x^2}{2\sigma^2}\right), \tag{15}$$

where $\Delta \equiv \frac{T_0 - T_\infty}{T_\infty}$ and $\sigma$ are the parameters characterizing the heating strength and width of the temperature profile, respectively. Using Eq. (10), the effective potential can be calculated to be

$$U_{eff}(x; n, \sigma, \Delta) = \frac{1}{2}\int_0^x \frac{n u^{n-1}}{1 + \Delta \exp\left[-\frac{u^2}{2\sigma^2}\right]} du + \ln\left(\frac{1 + \Delta e^{-\frac{x^2}{2\sigma^2}}}{1 + \Delta}\right). \tag{16}$$

The integral in (16) can be evaluated in terms of the polylogarithm function $\mathrm{Li}_k(z)$ and an explicit expression for $U_{eff}(x)$ can be derived analytically:

$$U_{eff}(x; n, \sigma, \Delta) = \frac{n\sigma^n}{2}\left[I_n(\frac{x}{\sigma}; \Delta) - I_n(0; \Delta)\right] + \ln\left(\frac{1 + \Delta e^{-\frac{x^2}{2\sigma^2}}}{1 + \Delta}\right), \tag{17}$$

$$\text{where} \qquad I_n(s; \Delta) = \sum_{k=1}^{n/2} (-1)^k \frac{(n-2)!!}{(n-2k)!!} s^{n-2k} \mathrm{Li}_k\left(-\frac{e^{\frac{s^2}{2}}}{\Delta}\right) \quad n = 2, 4, 6, \cdots \tag{18}$$

$$I_n(0; \Delta) = (-1)^{\frac{n}{2}} \mathrm{Li}_{\frac{n}{2}}\left(-\tfrac{1}{\Delta}\right). \tag{19}$$

The double-well structure in the effective barrier is characterized by the energy barrier, which can be derived from (17) to give

$$|E_{eff}(n, \sigma, \Delta)| = \frac{n\sigma^n}{2}\left[I_n(0; \Delta) - I_n\left(\frac{w(\sigma, \Delta)}{\sigma}; \Delta\right)\right] + \ln\left[\frac{1 + \Delta \exp\left[\frac{-w^2(\sigma,\Delta)}{2\sigma^2}\right]}{1 + \Delta}\right], \tag{20}$$

where $w = w(\sigma, \Delta)$ satisfies (using Eq. (11))

$$\frac{n\sigma^2}{2\Delta} = w^{2-n} \exp\left(-\frac{w^2}{2\sigma^2}\right). \tag{21}$$

$w(\sigma, \Delta)$ can further be solved explicitly from Eq. (21):

$$w(\sigma, \Delta) = \sigma\sqrt{2\ln\left(\tfrac{\Delta}{\sigma^2}\right)}, \quad n = 2 \tag{22}$$

$$= \sigma\sqrt{(n-2)\mathrm{W}\left(\frac{\left(\frac{2\Delta}{n\sigma^n}\right)^{\frac{2}{n-2}}}{n-2}\right)}, \quad n = 4, 6, 8, \cdots. \tag{23}$$

where W is the Lambert $W$ function. Notice that $\Delta > \sigma^2$ for $n = 2$ is the condition for forming an effective barrier for the case of a harmonic trap, which translates back to the dimensional form, reads $k_B T''(0) > k_{sp}$ ($k_{sp}$ is the stiffness of the harmonic trap), i.e. the local heating profile must be strong enough for the formation of the double-well structure in the effective potential. On the other hand, there is no such a condition for $n \geq 4$, and a double-well always exists in $U_{eff}$. The potential traps for $n = 2, 4, 6$ (solid curves) and the corresponding $U_{eff}(x)$ (dashed curves) for $T(x)$ given by (15) (dotted curve) are shown in Fig. 1a for $\sigma = 0.5$ and $\Delta = 1$, displaying the pronounced double-well features of $U_{eff}(x)$. The location of the wells in the effective potential (distance from the origin to the potential minimum) will vary as $n$, $\sigma$, or $\Delta$ changes, which is described by Eq. (22) or Eq. (23). The effective barrier varies with $\sigma$ and $\Delta$ for different $n$ as shown in Fig. 1b-1c. For smaller $\sigma$ or larger $\Delta$, the effective barrier becomes higher. As shown in the figure, the maximum $E_{eff}$ that can be achieved is determined by $\Delta$.

Next, we proceed to compute the transition rate between the double wells in $U_{eff}(x)$ using Eqs. (13) and (14). Using the $U_{eff}(x)$ in (17), one obtains

$$G(x,y) = \frac{n\sigma^n}{2}\left[I_n(\frac{y}{\sigma};\Delta) - I_n(\frac{x}{\sigma};\Delta)\right] - \ln\left(\frac{1+\Delta e^{-\frac{x^2}{2\sigma^2}}}{1+\Delta}\right), \tag{24}$$

and the transition rate can be computed numerically by evaluating the double integral in (13). One can also employ the steepest descent (saddle-point) method to derive an explicit approximation formula for $K^{-1}$, we obtain

$$K^{-1} \approx \frac{w(\sigma,\Delta)}{1+\Delta}\left[\sqrt{\frac{\pi}{2u''}}\left(\mathrm{erf}\left(\sqrt{\frac{u''}{2}}\right)+1\right) + \frac{1}{u''}\left(1-e^{-\frac{u''}{2}}\right)\right]\exp\left(E_{eff}\right), \tag{25}$$

where $E_{eff}$ is the effective barrier height given by (20), and $u'' \equiv U''_{eff}(w(\sigma,\Delta)) > 0$ is the curvature of the wells. The square bracket in Eq. (25) only depends on the curvature of the effective potential at $x = \pm w$. The exponential dependence of the transition rate on the barrier height is similar to the usual Kramers rate formula, albeit the dependence of the prefactor on the well curvature is significantly different. Using Eq. (17), one gets

$$u'' = \frac{2}{1+\sigma^2}\ln\frac{\Delta}{\sigma^2} \quad \text{for } n = 2 \tag{26}$$

$$= \frac{\sigma^{n-2}n(n-2)^{\frac{n}{2}}\left\{1+\mathrm{W}\left[\frac{1}{n-2}\left(\frac{2\Delta}{n\sigma^n}\right)\right]^{\frac{2}{n-2}}\right\}}{\sigma^n n(n-2)^{\frac{n-2}{2}} + 2\mathrm{W}\left[\frac{1}{n-2}\left(\frac{2\Delta}{n\sigma^n}\right)^{\frac{2}{n-2}}\right]^{\frac{2-n}{2}}}, \quad n = 4, 6, 8, \cdots \tag{27}$$

To verify the above theoretical results, we carry out Langevin dynamics simulations by numerically solving the Langevin equation using the Euler-Maruyama scheme with a time step of $10^{-4}$. The transition rate is measured from the first-passage times by averaging over $20,000$ trajectories. The steady-state position distribution is then measured, which in turn gives the effective potential. Fig. 1a (symbols) shows the effective potential measured in the simulations, which is in good agreement with the theoretical formula (17).

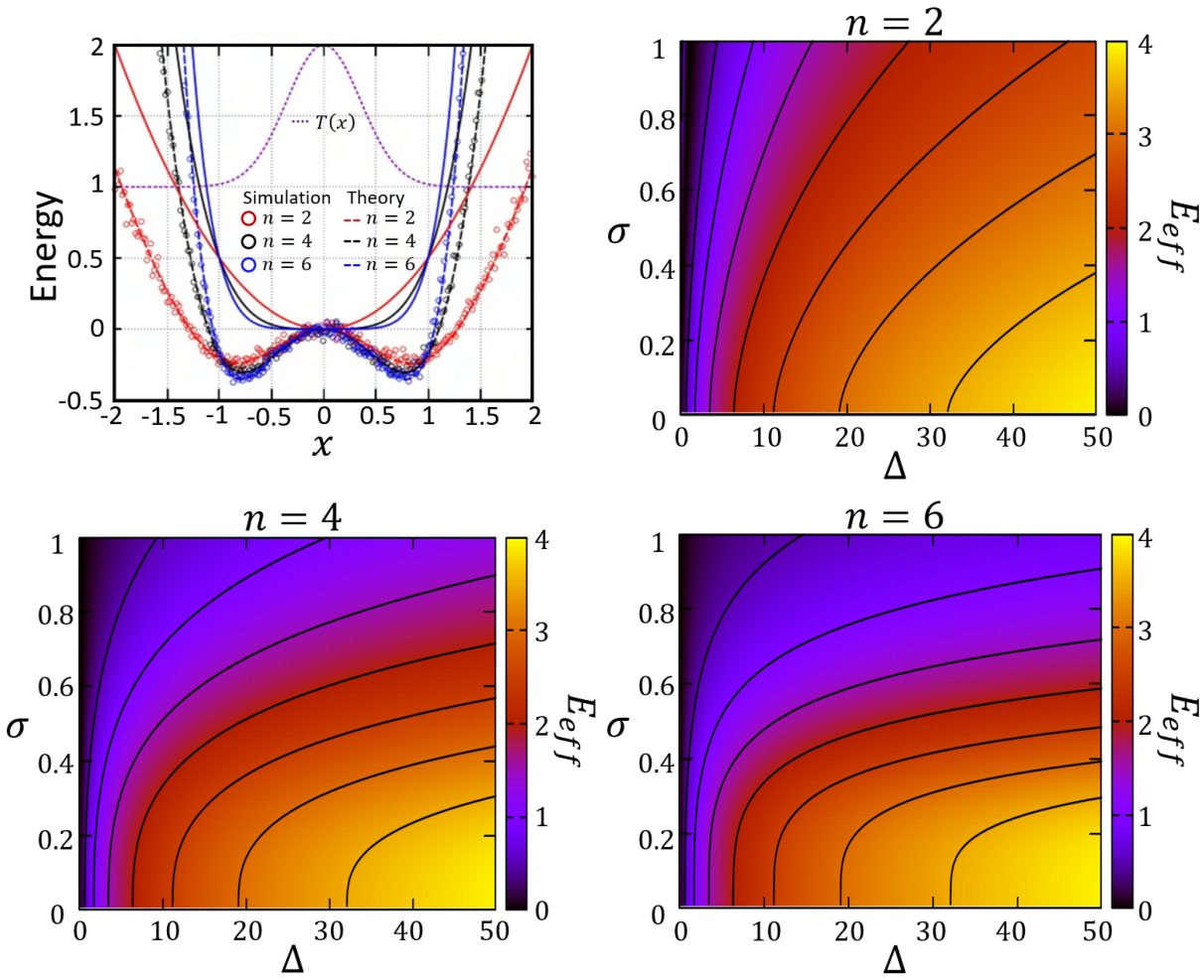


FIG. 1: (a) Double-well effective potentials $U_{eff}(x)$ (dashed curves) experienced by a Brownian particle under a Gaussian temperature field $T(x)$ (dotted curve) and various single-well harmonic and anharmonic potential traps (solid curves). $\sigma = 0.5$ and $\Delta = 1$. The effective potentials measured from simulations of the Langevin dynamics are also shown (symbols). (b)-(d) Contour plots of the effective barrier heights as a function of $\sigma$ and $\Delta$ for different trapping potentials of $n = 2, 4, 6$.

The mean first-passage time, whose inverse gives the transition rate between the wells in $U_{eff}$, can also be measured in the simulations. Fig. 2 shows the measured transition rates from simulations (symbols) for various trapping potentials of different values of $n$. As shown in Fig. 2a, $K$ decreases monotonically with the heating strength $\Delta$ for the $n = 2$ harmonic trap for a fixed value of $\sigma$, but displays a minimum with $\Delta$ for anharmonic traps. On the other hand, $K$ is non-monotonic with $\sigma$ and shows a minimum as $\sigma$ increases for a fixed value of $\Delta$ for harmonic and anharmonic traps, as shown in Fig. 2b. The measured transition rates all agree well with the theoretical formula (curves) given by (25).

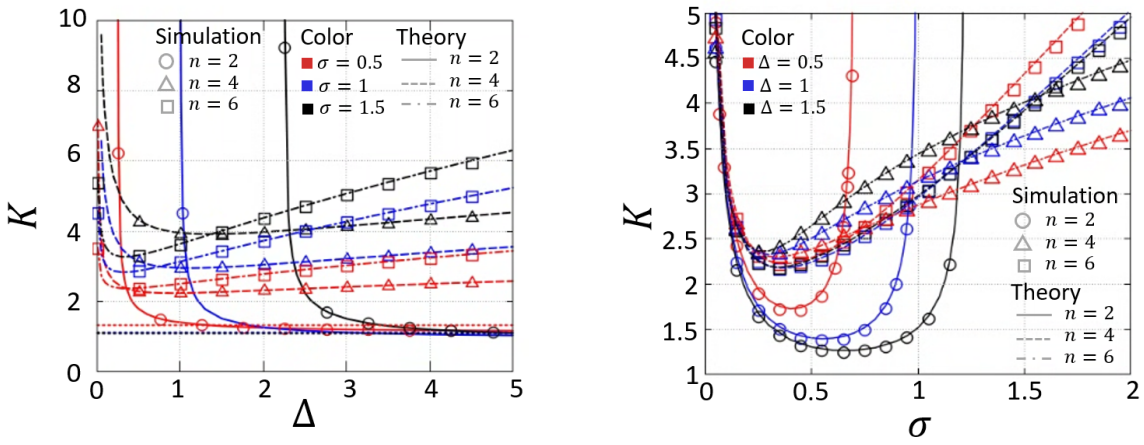


(a) (b)

FIG. 2: Transition rate in the double-well effective potential under different heating profiles. (a) $K$ vs. $\Delta$ for given values of $\sigma$. (b) $K$ vs. $\sigma$ for given values of $\Delta$. The symbols denote results from the Langevin simulations. The curves depict the theoretical results from numerical integration using (13).

The effective barrier varies with $\sigma$ or $\Delta$, but $\Delta$ dominates the possible maximum value of $E_{eff}$ as previously mentioned. Therefore, we select to fix $\sigma = 0.5$. The results are shown in Fig. 3a. It is worth noting that for the well-studied situation of a uniform temperature in a double-well potential trap, the Kramers rate formula indicates that the higher the potential barrier, the longer the escape time. However, in the present case of a double-well effective potential induced by a localized heating profile, the transition rate does not appear to follow anexponential decrease with the effective barrier height, in contrast ttoe usual Kramers rate result. This apparent disagreement is due to the fact that $E_{eff}$ arises from the non-uniform

temperature field and increases with $\Delta$, but at the same time, a larger $\Delta$ implies a higher temperature at $x = 0$, making it easier for the Brownian particle to escape from the trap. This effect is reflected in the prefactor $(1 + \Delta)$ in Eq. (25), and the results are shown in Fig. 3a. When $n = 4$ and $n = 6$, the $E_{eff}$ required for the minimum transition rate is much smaller than when $n = 2$. Moreover, the larger $n$ is, the larger the transition rate will be. To understand the effect of the induced barrier caused by the temperature gradient on the transition rate, we divide $K$ by the factor $(1 + \Delta)$, and the result is shown in Fig. 3b. The scaled transition rate effective barrier follows the usual Kramers' behavior of exponential decrease with the barrier height. In addition, the explicit approximation formula (25) (dashed curves) is a good approximation when $E_{eff}$ is large ($\gtrsim 1$), as shown in Fig. 3.

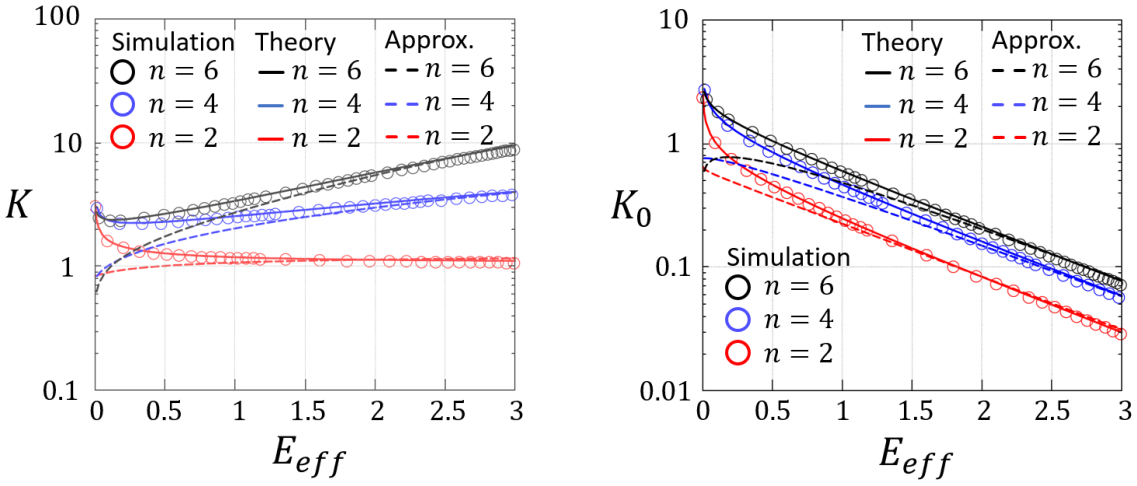


FIG. 3: (a) Transition rate for the double-well effective potential as a function of $E_{eff}$. $E_{eff}$ is varied by changing $\Delta$ while fixing $\sigma = 0.5$. The symbols denote results from the Langevin simulations, the solid curves depict results from numerical integration using (13), and the dashed curves present the approximation formula (25). The red, blue, and black colors represent $n = 2, 4, 6$ respectively. (b) After removing the influence of $\Delta$, the scaled effective transition rate reduces to a form similar to the usual Kramers' result.

## BROWNIAN PARTICLE TRAPPED BY A DOUBLE-WELL POTENTIAL AND UNDER A HEATING PROFILE: TUNING THE BARRIER AND TRANSITION RATE

In this section, we consider a double-well trapping potential and choose the double-well location (distance from the origin to the potential minimum) for the length unit. The dimensionless double-well potential is given by

$$U(x) = 4E_b\left(-\frac{1}{2}x^2 + \frac{1}{4}x^4\right), \tag{28}$$

where $E_b$ is the (dimensionless) barrier height. In the case of uniform temperature, the Brownian particle spends most of the time residing in one of the double wells and occasionally makes transitions to the other well under stochastic thermal fluctuations. In the presence of a nonuniform temperature field, the location of the wells of the effective potential and the effective barrier (and hence the transition rate between the wells) will be modified. For further calculations, we consider the Gaussian temperature profile also given by (15).

In this case, using (8), one can derive

$$U_{eff}(x; E_b, \sigma, \Delta) = 4E_b\int_0^x \frac{u^3 - u}{1 + \Delta\exp\left[-\frac{u^2}{2\sigma^2}\right]}du + \ln\left(\frac{1 + \Delta e^{-\frac{x^2}{2\sigma^2}}}{1+\Delta}\right), \tag{29}$$

$$= 4E_b\left[\sigma^4\left(I_4(\frac{x}{\sigma};\Delta) - I_4(0;\Delta)\right) - \sigma^2\left(I_2(\frac{x}{\sigma};\Delta) - I_2(0;\Delta)\right)\right] + \ln\left(\frac{1 + \Delta e^{-\frac{x^2}{2\sigma^2}}}{1+\Delta}\right), \tag{30}$$

and the effective energy barrier is given by

$$|E_{eff}(E_b, \sigma, \Delta)| = 4E_b\left[\sigma^2\left(I_2(\frac{1}{\sigma};\Delta) - I_2(0;\Delta)\right) - \sigma^4\left(I_4(\frac{1}{\sigma};\Delta) - I_4(0;\Delta)\right)\right] - \ln\left(\frac{1 + \Delta e^{\frac{-1}{2\sigma^2}}}{1+\Delta}\right). \tag{31}$$

Under the heating profile, the location of the double wells shifted from $x = \pm 1$ to $\pm w(E_b, \sigma, \Delta)$, which is given by

$$w(E_b, \sigma, \Delta) = \sqrt{2\sigma^2 \mathrm{W}\left[\frac{\Delta}{8E_b\sigma^4}e^{-\frac{1}{2\sigma^2}}\right] + 1}. \tag{32}$$

Note that $w \to 1$ if $\sigma \to 0$ or $\infty$, or $E_b \to \infty$. We then proceed to derive the transition rate and investigate how the rate $K$ is affected by the spatial temperature profile. Similar

to the case of a single well $U(x)$ in the previous section, the mean first-passage time and hence the inverse transition rate can be obtained by solving the backward Fokker-Planck equation. We obtain

$$K^{-1} \approx \exp(E_{eff})\sqrt{\frac{\pi}{2U''(1)}}\frac{1}{1+\Delta}\int_{-1}^{0}\exp\left[\frac{-|U''(0)|}{2T_0}y^2\right]\left(1+\mathrm{erf}\left(\sqrt{\frac{U''_{eff}(1)}{2}}(y+w)\right)\right)dy, \tag{33}$$

where $U''(0) = -4E_b$. We further employ the steepest-descent approximation for large $E_b$ to get

$$K^{-1} \approx \exp(E_{eff})\sqrt{\frac{\pi}{2U''(1)}}\frac{2}{1+\Delta}\int_{-\infty}^{0}\exp\left[\frac{-|U''(0)|}{2}y^2\right]dy \tag{34}$$

$$\Rightarrow K \approx \frac{1+\Delta}{\pi}\sqrt{U''_{eff}(1)|U''(0)|}\exp(-E_{eff}) \propto \exp(-E_b). \tag{35}$$

where $E_{eff}$ is the effective barrier given by (31). Eq. (35) is very similar to the expression of the Kramers rate, but the prefactor and exponent depend on the effective potential. Since $E_{eff}$ depends linearly on $E_b$, $K \sim e^{-E_b}$ as given by the r.h.s of (35). The dependences of the transition rate on the $\Delta$, $\sigma$, and $E_b$ are shown in Fig. 4, for both the theoretical results (curves) from (33) and those measured from Langevin simulations (symbols). Again, the theoretical formula agrees accurately with the simulation results. As shown in Fig. 4a, the transition rate increases with the temperature difference $\Delta$ for fixed values of $\sigma$ and $E_b$. This is expected since a stronger localized heating at the center will effectively lower the barrier of the double-well trap. Fig. 4b indicates that a smaller temperature gradient (larger $\sigma$ for a fixed value of $\Delta$) results in a higher transition rate, which saturates for $\sigma \gtrsim 2$. The transition rates as a function of the barrier of the double-well trap are displayed in Fig. 4c, verifying the exponential decrease with $E_b$ for $E_b \gtrsim 1$.

## TILTED DOUBLE-WELL EFFECTIVE POTENTIAL

For the case of a single well trapping potential such as the harmonic or anharmonic traps in (9), one can shift the center of the symmetric temperature profile to the location $x = a$, e.g., the heating laser beam is focused at $x = a$ and the temperature profile is modified to be

$$T(x) = 1 + \Delta e^{-\frac{(x-a)^2}{2\sigma^2}}. \tag{36}$$

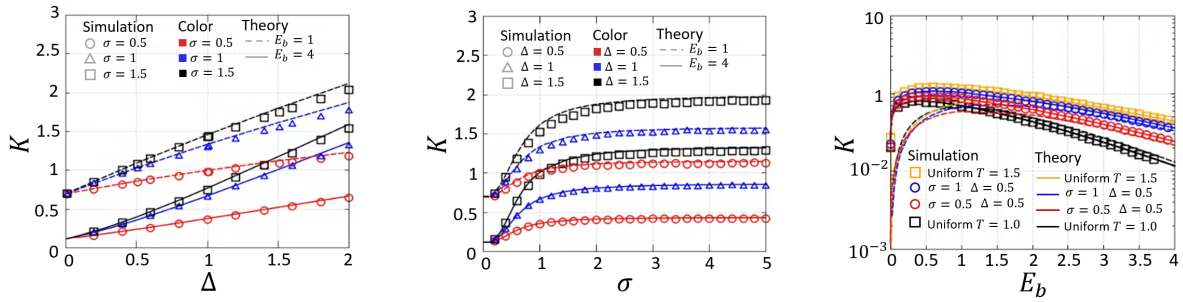


(a) (b) (c)

FIG. 4: Transition rate $K$ of a Brownian particle in a double-well trap under different heating profiles. Theoretical results (curves) are obtained using (33). $K$ measured from the Langevin simulation is denoted by the symbols. (a) $K$ vs. $\Delta$ for given $E_b$ and $\sigma$. (b) $K$ vs. $\sigma$ for given $E_b$ and $\Delta$. (c) $K$ vs. $E_b$ for various values of $\sigma$ and $\Delta = 0.5$. The transition rates for the cases of uniform temperatures of $T_0$ and $T_\infty$ are also shown for comparison.

The effective potential can be derived from (10) to give

$$U_{eff}(x) = \frac{n}{2}\int_{-a}^{x-a} \frac{\sum_{k=0}^{n-1} C_k^{n-1} u^{n-k-1} a^k}{1+\Delta\exp(\frac{-u^2}{2\sigma^2})} du + \ln\left[\frac{T(x)}{T(0)}\right] \tag{37}$$

$$= \frac{n}{2}\sum_{k=0}^{n-1} C_k^{n-1} a^k \left\{\int_{-a}^{x-a} \frac{u^{n-k-1}}{1+\Delta\exp(\frac{-u^2}{2\sigma^2})} du\right\} + \ln\left[\frac{T(x)}{T(0)}\right] \tag{38}$$

$$= \frac{n}{2}\sum_{k=0}^{n-1} C_k^{n-1} a^k \sigma^{n-k} \left\{I_{n-k}(\frac{x-a}{\sigma};\Delta) - I_{n-k}(-\frac{a}{\sigma};\Delta)\right\} + \ln\left[\frac{T(x)}{T(0)}\right], \tag{39}$$

where $I_n(s;\Delta)$ is given by (18). Fig. 5a plots $U_{eff}(x)$ for the harmonic trap under a temperature field centered at $x = a$ for various values of $a$, showing that the double-well in the effective potential is tilted. The dependence of the tilted double-well effective potential also depends on the heating profile characterized by $\sigma$ and $\Delta$ as shown in Fig. 5b and 5c. One can easily see that as the heating profile is farther away from the potential trap center, the effective potential is more tilted, and eventually the effective barrier vanishes as $|a|$ becomes sufficiently large. The analytic expression of $U_{eff}(x)$ given by (39) is verified by measuring the steady-state position distribution from Langevin simulations, and the results are also shown in Fig. 5a to 5c (the symbols), showing good agreement.

Such a tilted double-well effective potential can be obtained by mismatching the centers of the trapping well and the temperature profile, opening the possibility of constructing a

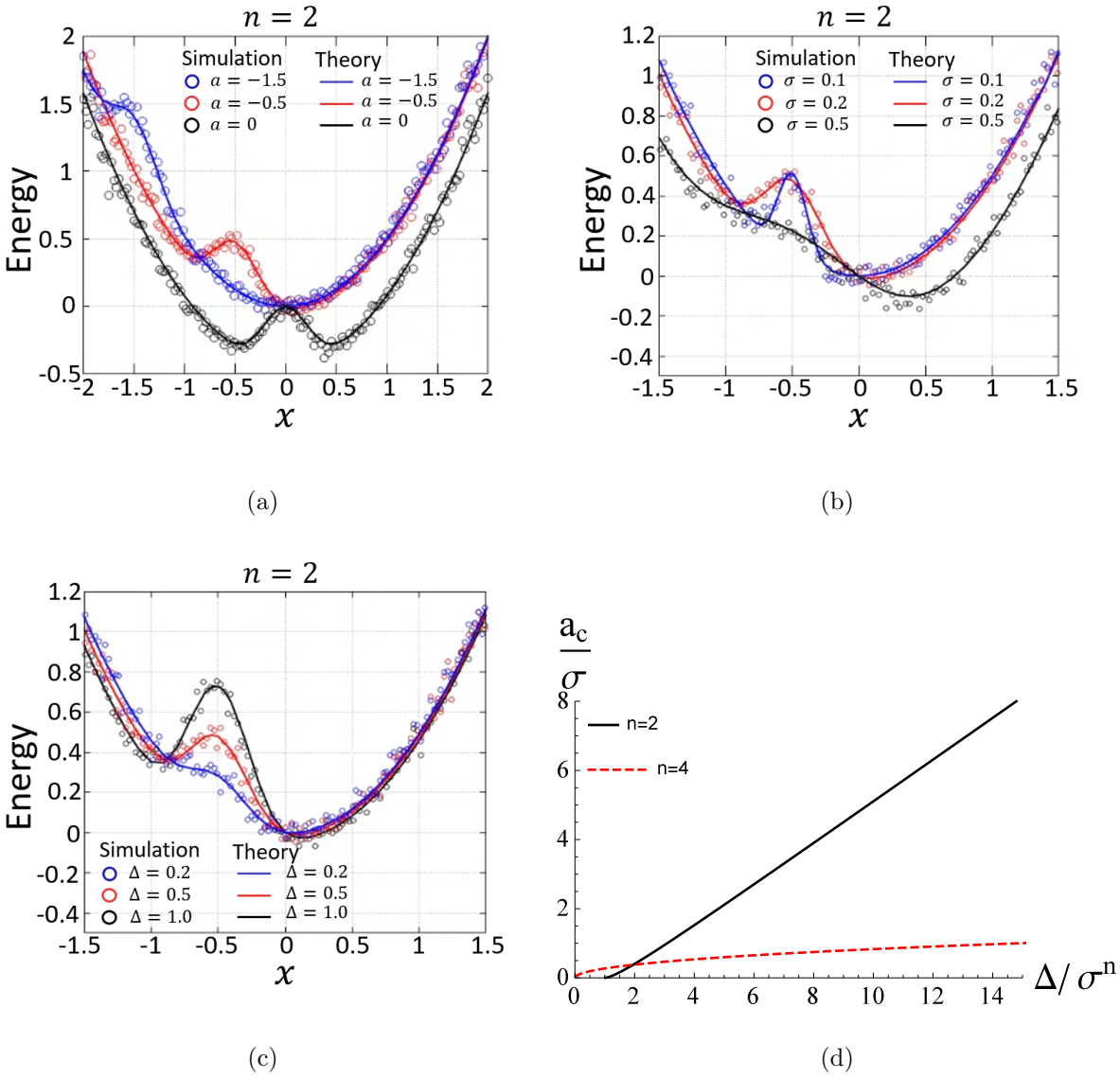


FIG. 5: The dimensionless effective potential $U_{eff}(x)$ calculated using (10) for the harmonic trap centered at $x = 0$ subjected to the temperature profile centered at $x = a$ as given by (36). (a) $\sigma = 0.2$ and $\Delta = 0.5$ for various values of $a$. (b) $a = -0.5$ and $\Delta = 0.5$ for various values of $\sigma$. (c) $a = -0.5$ and $\sigma = 0.2$ for various values of $\Delta$. (d) The critical $\tilde{a}_c \equiv a_c/\sigma$ plotted as a function of $\frac{\Delta}{\sigma^n}$ for the $n = 2$ and $n = 4$ traps, obtained from the solution of (40) and (41). The off-center heating profile is at the positive $x$ location.

memory erasure device in such a system. The critical value of the off-center distance, $a_c$ can be determined from the condition of the inflexion point of $U_{eff}(x)$, namely $U'_{eff}(x) = U''_{eff}(x) = 0$ from which the inflexion point $x_c$ and the critical value $a_c$ can be solved. The

inflexion point conditions, in terms of $\tilde{x} \equiv x/\sigma$ and $\tilde{a} \equiv a/\sigma$, can be simplified to

$$\frac{n}{2}\tilde{x}^{n-1} = \frac{\Delta}{\sigma^n}(\tilde{x}-\tilde{a})e^{-\frac{(\tilde{x}-\tilde{a})^2}{2}} \tag{40}$$

$$(n-1)(\tilde{x}-\tilde{a}) = \tilde{x}\left[1-(\tilde{x}-\tilde{a})^2\right], \tag{41}$$

whose root gives the inflexion point $\tilde{x}_c$ and the critical $\tilde{a}_c$. Note that both $\tilde{x}_c$ and $\tilde{a}_c$ depend only on $\Delta/\sigma^n$ and $n$. Fig. 5d shows $\tilde{a}_c$ as a function of $\Delta/\sigma^n$ for the harmonic and anharmonic traps for $a > 0$ off-center heating. There is a similar negative $\tilde{a}_c$ branch for the $a < 0$ off-center heating (not shown). One can design appropriate protocols that move the heating center to achieve efficient erasure with low dissipation.

## DOUBLE-WELL POTENTIAL AND GAUSSIAN TEMPERATURE PROFILE

The potential and temperature are given by (28) and (36). Then, the effective potential can be written as

$$U_{eff}(x) = 4E_b \int_0^x \frac{-s+s^3}{1+\Delta\exp\left(\frac{-(s-a)^2}{2\sigma^2}\right)}ds + \ln\left[\frac{T(x)}{T(0)}\right]. \tag{42}$$

Leaving $u = s - a$ and $du = ds$, we obtain

$$U_{eff} = 4E_b \int_{-a}^{x-a} \frac{-(u+a)+(u+a)^3}{1+\Delta\exp\left(\frac{-u^2}{2\sigma^2}\right)}du + \ln\left[\frac{T(x)}{T(0)}\right]. \tag{43}$$

Taking the derivative of Eq. (42) for $x$, we obtain the following equations.

$$\left(x^3-x\right) = C\frac{x-a}{\sigma^2}e^{-\frac{(x-a)^2}{2\sigma^2}} \tag{44}$$

$$\left(\sigma^2-(x-a)^2\right)\left(x^3-x\right) = \left(3x^2-1\right)(x-a)\,\sigma^2, \tag{45}$$

where $C \equiv \frac{\Delta}{4E_b}$. Eqs. (44) and (45) have at most 5 roots, which means $U_{eff}(x)$ have at most 3 wells. Fig. 6a and b are generated by solving Eqs. (44) and (45), where $a_c$ means that when $\Delta$ and $\sigma$ are given, what the value of $a$ is required to satisfy Eqs. (44) and (45). We refer to $a_c$ as the critical value of $a$ because it always occurs when the number of wells is different. It should be noted that $a_c$ may have multiple values. To avoid the third well, the value of $a$ should not be chosen within the area enclosed by the curve $a_c$, except for the color area, indicating that $U_{eff}(x)$ has only 1 well. The area outside the curve indicates the condition for 2 wells of $U_{eff}(x)$. As shown in the Fig. 6a, to produce only 1 well, $C$ should

be greater than about 0.284. Fig. 6b shows that $a_c$ varies with $C$. We plot the profile of the effective potential, and the range of $a$ that can produce 1 well when $\sigma = 0.5$ and $C = 0.5$ in Fig. 7. Experimentally, the effective barrier can be removed by selecting an appropriate set of parameters.

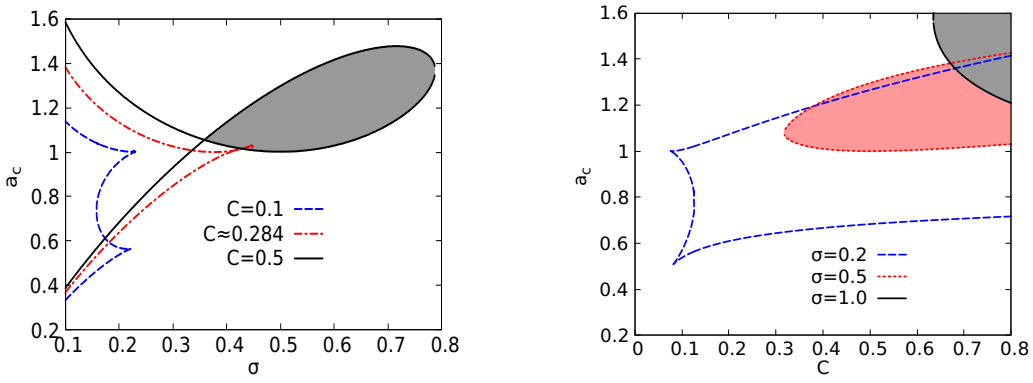


(a) (b)

FIG. 6: (a) The critical value $a_c$ varies with $\sigma$. The curves can be divided into three situations, as shown in the figure. Within the region enclosed by the curves, the effective potential contains three wells. In the black region, however, there is only one well. Outside the curves, the effective potential has two wells. (b) The critical value $a_c$ varies with $C$. Within the region enclosed by the curves, the effective potential contains three wells. In the color region, however, there is only one well. Outside the curves, the effective potential has two wells.

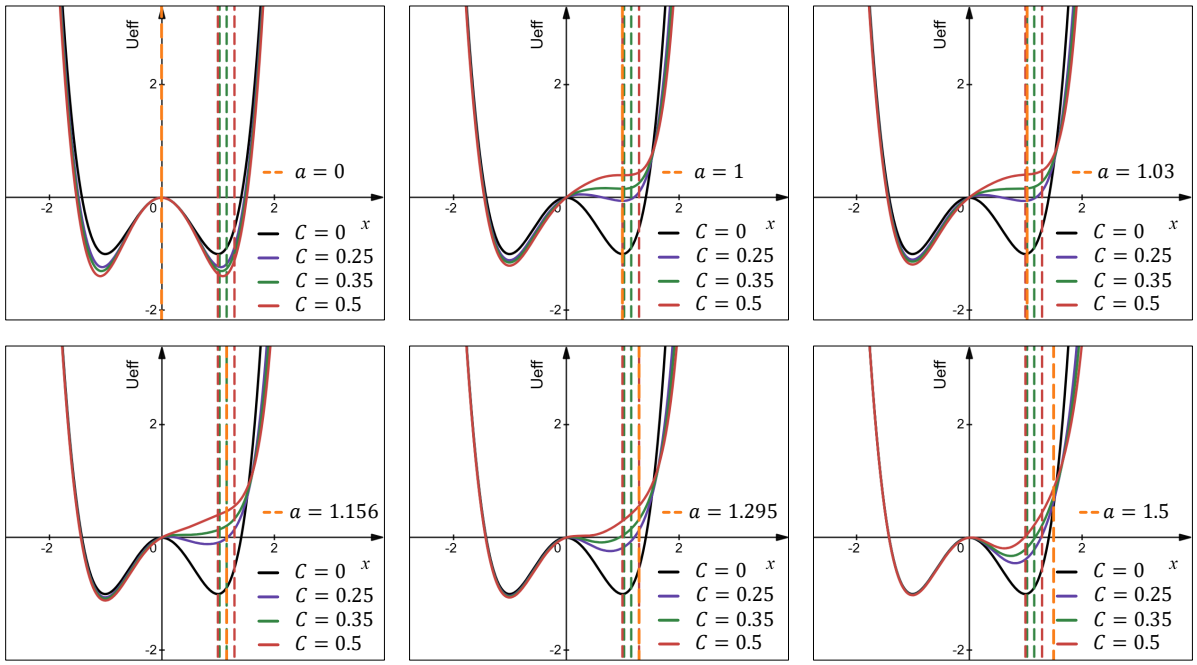


(a)

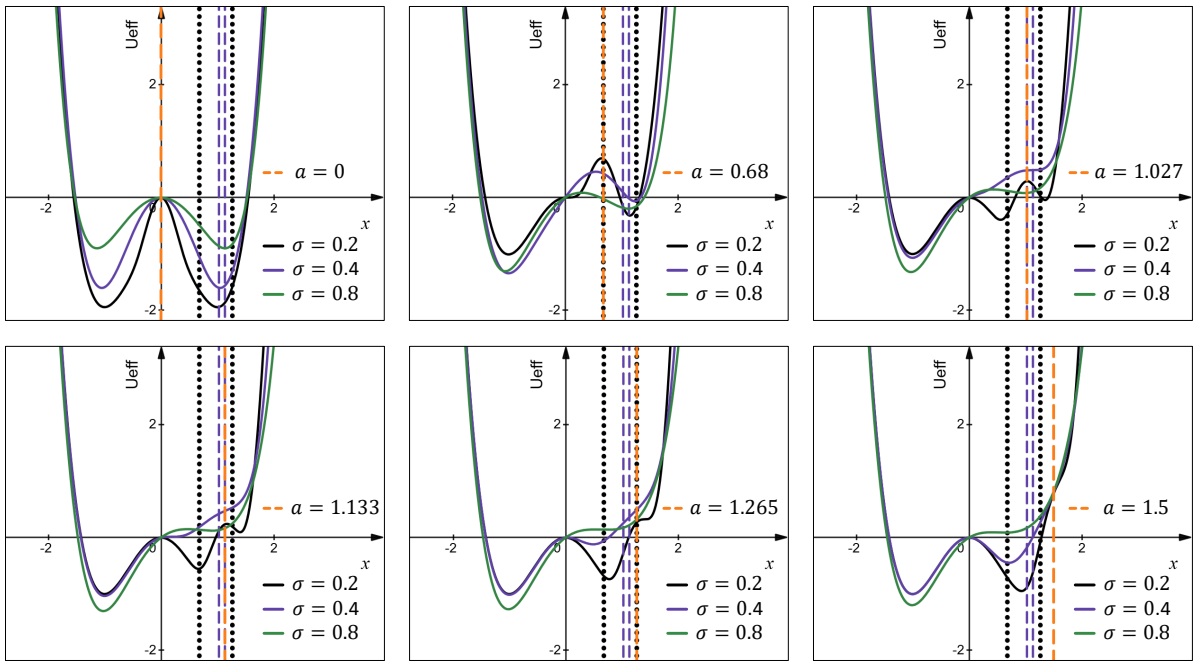


(b)

FIG. 7: (a) The theoretical shape of $U_{eff}$ (solid curves) varies with $C$ and $a$, where $\sigma = 0.5$ is fixed. (b) The theoretical shape of $U_{eff}$ (solid curves) varies with $\sigma$ and $a$, where $C = 0.5$ is fixed. The orange dashed line represents the value of $a$ in both figures. The area between the dashed lines is the range of $a$ values that can produce only 1 well for different $U_{eff}$, while $a$ between the dotted lines represents $U_{eff}$ has 3 wells.

**Optimization protocol for varying temperature field: minimum heat cost in a finite time or minimum entropy production**

The first law of thermodynamics is given by $\dot{E} = \dot{Q} + \dot{W}$, where $E$ is the internal energy, $Q$ is the heat, and $W$ is the work done to the system. The internal energy can be written as

$$E(t) = \int_{-\infty}^{\infty} U(x,t)P(x,t)dx. \tag{46}$$

We then have,

$$\dot{E}(t) = \int_{-\infty}^{\infty} \left[\frac{\partial U(x,t)}{\partial t}P(x,t) + \frac{\partial P(x,t)}{\partial t}U(x,t)\right] dx \tag{47}$$

$$= \dot{W}(t) + \dot{Q}(t). \tag{48}$$

The entropy of a system is defined by

$$S_{sys}(t) = -k_B \int_{-\infty}^{\infty} P(x,t)\ln(P(x,t))dx. \tag{49}$$

Heat flows into the system is given by

$$Q(t) = \int_0^t \dot{Q}(s)ds = \int_0^t \int_{-\infty}^{\infty} \frac{\partial P(x,s)}{\partial t}U(x,s)dxds. \tag{50}$$

Using the Fokker-Planck equation, one gets

$$Q(t) = -\int_0^t \int_{-\infty}^{\infty} \frac{\partial J(x,s)}{\partial x}U(x,s)dxds \tag{51}$$

$$= -\int_0^t \cancelto{0}{\left[\frac{\partial J(x,s)}{\partial x}U(x,s)\right]_{x=-\infty}^{\infty}} ds + \int_0^t \int_{-\infty}^{\infty} \frac{\partial U(x,s)}{\partial x}J(x,s)dxds \tag{52}$$

$$= -\int_0^t \int_{-\infty}^{\infty} \frac{J(x,s)\gamma(x,s) + \frac{\partial}{\partial x}\left(k_B T(x,s)P(x,s)\right)}{P(x,s)}J(x,s)dxds \tag{53}$$

$$= -\int_0^t \int_{-\infty}^{\infty} P(x,s)v^2(x,s)\gamma(x,s)dxds$$
$$- k_B \int_0^t \int_{-\infty}^{\infty} J(x,s)T(x,s)\frac{\partial}{\partial x}\left[\ln(P(x,s))\right]dxds - k_B \int_0^t \int_{-\infty}^{\infty} J(x,s)\frac{\partial T(x,s)}{\partial x}dxds \tag{54}$$

$$= -\int_0^t \int_{-\infty}^{\infty} P(x,s)v^2(x,s)\gamma(x,s)dxds - k_B \int_0^t \int_{-\infty}^{\infty} T(x,s)\frac{\partial\left[P(x,s)\ln P(x,s)\right]}{\partial s}dxds$$
$$+ k_B \int_0^t \int_{-\infty}^{\infty} \frac{\partial T(x,s)}{\partial x}v(x,s)P(x,s)\ln P(x,s)dxds. \tag{55}$$

The first term is the standard friction dissipation. The second term is similar to the system entropy multiplied by the differently weighted temperature $T(x,t)$, while the third term is the coupling term of the information entropy and the temperature gradient. The third term appears to be insensitive to the speed of the erasure protocol, as $v(x,t)$ is linear. Therefore, the Landauer bound is given by the first and third terms.

If $T$ is a constant, the second term is independent of the protocol, and the third term is 0, therefore, we only need to do the variation on the first term to find the optimal protocol. However, in the most general case (both $T$ and $U$ can vary over time), all three terms are related to the path.

We first assume that $\gamma$ is a constant. The optimization function equation for the first term is derived in [24, 25].

$$\delta Q_1(t) = \int_0^t \int_{-\infty}^{\infty} 2\gamma \left[ \partial_t \left( \frac{\dot{f}}{f'} \right) - \frac{\dot{f}}{f'} \partial_x \left( \frac{\dot{f}}{f'} \right) \right] \delta f dx ds, \tag{56}$$

where $f(x,t) \equiv \int_{-\infty}^{x} P(z,t) dz$. We suggest combining the second and third terms to perform the variation.

$$Q_2(t) + Q_3(t) = k_B \int_0^t \int_{-\infty}^{\infty} T(x,s) P(x,s) \partial_x v(x,s) dx ds \tag{57}$$

$$= -k_B \int_0^t \int_{-\infty}^{\infty} T(x,s) f' \partial_x \left( \frac{\dot{f}}{f'} \right) dx ds. \tag{58}$$

Thus,

$$\mathcal{L}(T, f, f') \equiv T f' \partial_x \left( \frac{\dot{f}}{f'} \right) \tag{59}$$

## NONEQUILIBRIUM STEADY-STATE: UNDERDAMPED DYNAMICS AND HIDDEN ENTROPY PRODUCTION DUE TO TEMPERATURE GRADIENT

The one-dimensional overdamped Fokker-Planck equation leads to the zero particle flux condition, and hence suggests an equilibrium picture (and hence the vanishing entropy production) even in the presence of a temperature gradient. The above paradoxical result is due to the hidden entropy production in the coarse-graining of the degree of freedom of fast momentum[26, 27]. To see explicitly the non-equilibrium nature of the system due to the temperature gradient, one needs to consider the underdamped Langevin dynamics for

the heat transfer because of the unavoidable kinetic energy transport due to momentum transfer in the presence of temperature variations. The underdamped Langevin dynamics of a Brownian particle of mass $m$ and momentum $p$ is given by

$$\dot{x} = \frac{p}{m} \tag{60}$$

$$\dot{p} = -U'(x) - \frac{\gamma p}{m} + \sqrt{2\gamma k_B T(x)}\xi(t). \tag{61}$$

Notice that in the presence of the inertia, the variation of $x(t)$ in $dt$ is $\mathcal{O}(dt)$, in contrast to the overdamped case of $\mathcal{O}(\sqrt{dt})$. Hence, the multiplicative nature of the noise in (61) causes no ambiguities, and there is no distinction between the Ito or Stratonovich convention in the underdamped Langevin dynamics[23]. (60) and (61) can be put in dimensionless form as[28, 29]

$$\dot{x} = p, \quad \alpha\dot{p} = -p - U'(x) + \sqrt{2T(x)}\xi(t), \tag{62}$$

where $\alpha \equiv \tau_m/\tau_R$ with $\tau_m = m/\gamma$ is the inertial time and $\tau_R = \frac{\gamma}{k_B T_\infty}\left(\frac{k_B T_\infty}{\lambda}\right)^{2/n}$ is the relaxation time in the trap (which is also the time unit we chose). The stochastic heat can be calculated as (in dimensionless form) $dQ = \frac{\alpha}{2}dp^2 + U'(x) \circ dx$, and the stochastic entropy production to the environment is given by

$$dS_{env} = -\frac{\alpha p}{T(x)} \circ dp - \frac{U'(x)}{T(x)} \circ dx. \tag{63}$$

The mean entropy production rate is given by the mean hidden (or anomalous) entropy production rate due to the temperature gradient, which has been derived in [26]. Following similar calculations, the mean entropy production rate to the environment is derived to be (in dimensionless form)

$$\langle \dot{S}_{env} \rangle = \frac{1}{2}\left\langle \frac{T'(x)^2}{T(x)} \right\rangle = \frac{\int_{-\infty}^{\infty} \frac{T'(x)^2}{T(x)} e^{-U_{eff}(x)} dx}{2\int_{-\infty}^{\infty} e^{-U_{eff}(x)} dx}. \tag{64}$$

Underdamped Langevin dynamics simulations are performed by solving (60) and (61) numerically. The position distribution function and hence the effective potential are measured as shown in Fig. 8a. For small values of $\alpha$, the effective potential obtained from the underdamped Langevin simulations agrees well with the theoretical result derived from (1), indicating that the overdamped Fokker-Planck equation can faithfully describe the Brownian particle position statistics.

The steady-state average entropy production rate to the environment is also measured from the simulations as shown in Fig. 8b, indicating that there is a finite entropy production rate even in the overdamped limit of small $\alpha$, manifesting the nonquilibrium nature of the system due to the temperature gradient. The steady-state $\langle \dot{S}_{env} \rangle$ increases with the temperature gradient as shown in Fig. 8c for both the underdamped case and in the overdamped limit of $\alpha = 0.01$. Furthermore, the theoretical result of $\langle \dot{S}_{env} \rangle$ given by (64) is in excellent agreement with the simulation results for the overdamped case.

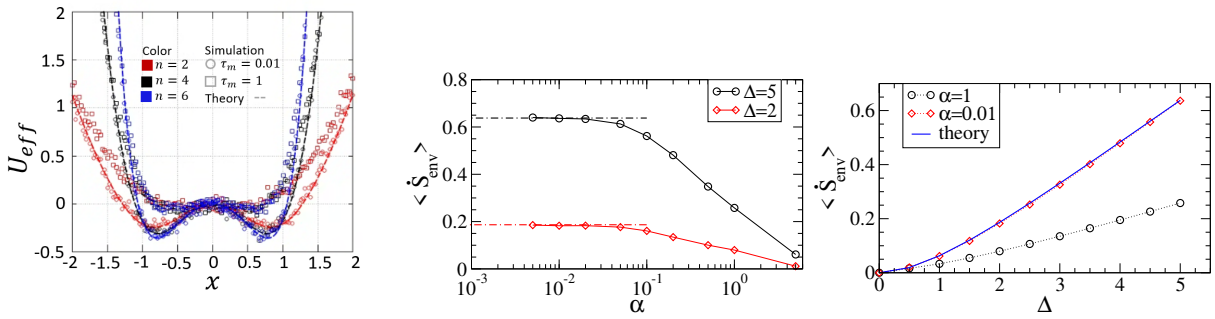


(a) (b) (c)

FIG. 8: Langevin dynamics simulation of the underdamped Brownian particle under a potential trap and the temperature field (15). (a) The effective potentials measured from the steady-state position distributions for $n = 2, 4, 6$ potential traps and $\alpha = 1$ and 0.01. $\sigma = 0.5$. The theoretical $U_{eff}(x)$ in the overdamped limit are shown by the dashed curves. (b) The steady-state average entropy production rate to the environment, $\langle \dot{S}_{env} \rangle$, measured from the simulations vs. $\alpha \equiv \frac{\tau_m}{\tau_\alpha}$ for harmonic trap under $T(x)$ with $\sigma = 1$ and $\Delta = 2$ and 5. The theoretical values in the overdamped limit given by (64) are marked by the horizontal dot-dashed lines. (c) Measured $\langle \dot{S}_{env} \rangle$ vs. $\Delta$ with $\sigma = 1$ for $\alpha = 1$ and 0.01. The theoretical overdamped result given by (64) is shown by the solid blue curve.

## CONCLUSION AND OUTLOOK

In this paper, we consider the Brownian particle in a one-dimensional potential well and under a single-peak temperature field. The system can be described by an effective potential, which can consist of an effective potential barrier. Thus, the transition rate can be manipulated by the imposed temperature field. Explicit analytic formulae for the effective

potentials are derived (Eqs. (17), (39), and (30)). In addition, following the Kramers' approach, we derive approximate formulas of the transition rates (Eqs. (25) and (35)). A challenging question is whether such a system with an emerged effective barrier can store information like an ordinary double-well potential. If so, what determines the corresponding Landauer limit of such systems with nonuniform temperatures? It may be possible to store information for a short period of time, but the ability to store information might not be stable enough, and it may be challenging to discuss the relevant Landauer limit.

For motion in higher spatial dimensions or Brownian systems with more degrees of freedom described by $\vec{x}$, the zero particle flux condition cannot be achieved in general. This can be seen if one imposes the zero flux condition in the corresponding Fokker-Planck equation in (2), which gives the steady-state distribution as

$$P(\vec{x}) \sim \frac{1}{T(\vec{x})} \exp\left(-\int^{\vec{x}} \frac{\nabla U(\vec{x}') \cdot d\vec{x}'}{T(\vec{x}')}\right), \tag{65}$$

but the integral on the rhs is in general path-dependent, implying the zero flux condition will not hold in general. On the other hand, if the temperature field is chosen to satisfy $T(\vec{x}) = f(U(\vec{x}))$ everywhere for some function $f$, then one can easily verify that $\nabla T \times \nabla U = 0$ everywhere, and the no particle flux condition is fulfilled. In this case, an effective potential can be obtained for higher dimensions:

$$U_{eff}(\vec{x}) = \int^{U(\vec{x})} \left[\frac{1 + f'(V)}{f(V)}\right] dV \quad \text{if } T(\vec{x}) = f(U(\vec{x})), \tag{66}$$

with the steady-state distribution $P_{ss}(\vec{x}) \sim e^{-U_{eff}(\vec{x})}$. It remains a challenge to calculate theoretically the nonequilibrium steady state distribution under a general non-uniform $T(\vec{x})$ with a nonvanishing flux $\vec{J}_{ss}(\vec{x})$ in higher dimensions.

**Acknowledgment:** This work has been supported by the National Science and Technology Council of Taiwan under grant no. 113-2112-M008-018-MY2.

[1] Herbert B Callen. *Thermodynamics and an Introduction to Thermostatistics*. John wiley & sons, 1985.

[2] C. Soret. Sur l'état d'équilibre que prend, au point de vue de sa concentration, une dissolution saline primitivement homogène, dont deux parties sont portées à des températures différentes. *J. Phys. Theor. Appl.*, (9):331, 1879.

[3] Miki Matsuo and Shin-ichi Sasa. Stochastic energetics of non-uniform temperature systems. *Physica A: Statistical Mechanics and its Applications*, 276(1-2):188–200, 2000.

[4] M. von Smoluchowski. Experimentell nachweisbare, der ublichen thermodynamik widersprechende molekularphenomene. *Phys. Zeitshur.*, 13:1069, 1912.

[5] Richard Phillips Feynman, Robert B Leighton, and Matthew Sands. Lectures on physics, vol. 1, chapter 46, 1963.

[6] Jaehoon Bang, Rui Pan, Thai M Hoang, Jonghoon Ahn, Christopher Jarzynski, HT Quan, and Tongcang Li. Experimental realization of Feynman's ratchet. *New Journal of Physics*, 20(10):103032, 2018.

[7] B¨uttiker M. Transport as a consequence of state-dependent diffusion. *Phys. B: Condens. Matter*, (68):161, 1987.

[8] Landauer R. Motion out of noisy states. *J. Stat. Phys.*, (53):233, 1988.

[9] Roger Filliger and Peter Reimann. Brownian Gyrator: A Minimal Heat Engine on the Nanoscale. *Physical Review Letters*, 99(23):230602, dec 2007.

[10] K-H Chiang, C-L Lee, P-Y Lai, and Y-F Chen. Electrical autonomous brownian gyrator. *Physical Review E*, 96(3):032123, 2017.

[11] Hsin Chang, Chi-Lun Lee, Pik-Yin Lai, and Yung-Fu Chen. Autonomous brownian gyrators: A study on gyrating characteristics. *Physical Review E*, 103(2):022128, 2021.

[12] Albert Einstein. Über die von der molekularkinetischen Theorie der Wärme geforderte Bewegung von in ruhenden Flüssigkeiten suspendierten Teilchen. *Annalen der physik*, 322(8):549–560, 1905.

[13] Jean Perrin. Mouvement brownien et réalité moléculaire. *Ann. Chim. Phys.*, 18:1, 1909.

[14] G. E. Uhlenbeck and L. S. Ornstein. On the Theory of the Brownian Motion. *Phys. Rev.*, 36(5):823–841, September 1930.

[15] Hannes Risken. *The Fokker-Planck equation: methods of solution and applications*. Springer, Berlin, 2nd ed. edition, 1989.

[16] Paul Langevin. Sur la théorie du mouvement brownien. *Comptes Rendus de l'Academie des Sciences*, 146:530–533, 1908.

[17] Ken Sekimoto. *Stochastic Energetics*, volume 799 of *Lecture Notes in Physics*. Springer Berlin Heidelberg, Berlin, Heidelberg, 2010.

[18] Udo Seifert. Stochastic thermodynamics, fluctuation theorems and molecular machines. *Re-*

*ports on progress in physics. Physical Society (Great Britain)*, 75(12):126001, dec 2012.

[19] Peter Hänggi, Peter Talkner, and Michal Borkovec. Reaction-rate theory: fifty years after kramers. *Reviews of modern physics*, 62(2):251, 1990.

[20] Jakub Spiechowicz, Ivan G. Marchenko, Peter Hänggi, and Jerzy Łuczka. Diffusion coefficient of a brownian particle in equilibrium and nonequilibrium: Einstein model and beyond. *Entropy*, 25(1), 2023.

[21] Yusheng Shen, Chengjie Luo, Yan Wen, Wei He, Pingbo Huang, Hsuan-Yi Chen, Pik-Yin Lai, and Penger Tong. Directed motion of membrane proteins under an entropy-driven potential field generated by anchored proteins. *Phys. Rev. Res.*, 3:043195, Dec 2021.

[22] N.G. van Kampen. Diffusion in inhomogeneous media. *Z. Physik B - Condensed Matter*, 68:135–138, 1987.

[23] Miki Matsuo and Shin-ichi Sasa. Stochastic energetics of non-uniform temperature systems. *Physica A: Statistical Mechanics and its Applications*, 276(1):188–200, 2000.

[24] Yunxin Zhang. Work needed to drive a thermodynamic system between two distributions. *Europhysics Letters*, 128(3):30002, 2020.

[25] Karel Proesmans, Jannik Ehrich, and John Bechhoefer. Optimal finite-time bit erasure under full control. *Physical Review E*, 102(3):032105, 2020.

[26] Antonio Celani, Stefano Bo, Ralf Eichhorn, and Erik Aurell. Anomalous thermodynamics at the microscale. *Phys. Rev. Lett.*, 109:260603, Dec 2012.

[27] Kyogo Kawaguchi and Yohei Nakayama. Fluctuation theorem for hidden entropy production. *Phys. Rev. E*, 88:022147, Aug 2013.

[28] Yonggun Jun and Pik-Yin Lai. Instantaneous equilibrium transition for brownian systems under time-dependent temperature and potential variations: Reversibility, heat and work relations, and fast isentropic process. *Phys. Rev. Res.*, 3:033130, Aug 2021.

[29] Yonggun Jun and Pik-Yin Lai. Minimal dissipation protocols of an instantaneous equilibrium brownian particle under time-dependent temperature and potential variations. *Phys. Rev. Res.*, 4:023157, May 2022.